CFD Output Data Checking for Kirchhoff Rotor Noise Applications

J. J. Lasserre*, C. Polacsek,

Office National d'Etudes et de Recherches Aérospatiales, BP72, 92322 Châtillon Cedex, France

* Present address: Institut de Recherche des Phénomènes Hors Equilibre, 12 avenue du Général Leclerc, 13003 Marseille, France.

Abstract

An investigation to assess the reliability of aerodynamic data used as direct or non-direct inputs in Kirchhoff rotor noise methods is proposed in this paper. Simple and efficient criterion are presented and applied to high-speed impulsive noise configurations with shock delocalization. Through a parametrical study on Kirchhoff surface radius, CFD output data analyses are related to the accuracy of the acoustic predictions, compared to experiment. Thus, advices for the extent and position of the control surface are given and the validity domain of the CFD/Kirchhoff method presented here is clearly addressed.

Introduction

Recent progress in CFD has made new aeroacoustic methods applicable for predicting helicopter rotor noise, in particular for high-speed impulsive noise and blade-vortex interaction noise. Kirchhoff theory has been reviewed by acousticians in order to develop formulations suited to their problems. Because of its simplicity, the Kirchhoff method, based on a surface integration, has been preferred to the Lighthill's acoustic analogy, which requires a volume integration if quadrupoles are present. However, the validity of such a method is mainly related to the hypothesis of linear Kirchhoff formulations mainly adopted [1-5]. It assumes the control surface to surround all the non linear domain including the acoustic sources and so to be located far enough from the rotor. In another hand, most of numerical schemes are diffusive causing dissipation effects which increase with the distance to the rotor because of the increase of the size of the cells. This problem is emphasized by the difficulty to accurately capture the shock wave up to the boundaries of the mesh, in particular when using a structured grid [6, 7]. For these reasons, it is not safe to put the control surface too far from the rotor. A compromise has then to be found in order to satisfy to these restrictions.

To illustrate this problem, a theoretical range for the location of a cylindrical Kirchhoff surface is presented in Figure 1, where $\hat{E}$ is an estimator function measuring the accuracy of the method (optimal when $\hat{E} = 1$), and R_{k1} and R_{k2} are the limits of the valid domain.

The paper aims to assess the limits of that domain for the CFD/Kirchhoff method used here. The validity of the input data for the Kirchhoff method is checked through several parameters such as the pressure normal derivative, the acoustic intensity , or the sound celerity analysis. Computations are applied to high-speed configurations, including shock delocalization, relative to model rotors with rectangular blades for which computed acoustic signatures can be compared to experiment.

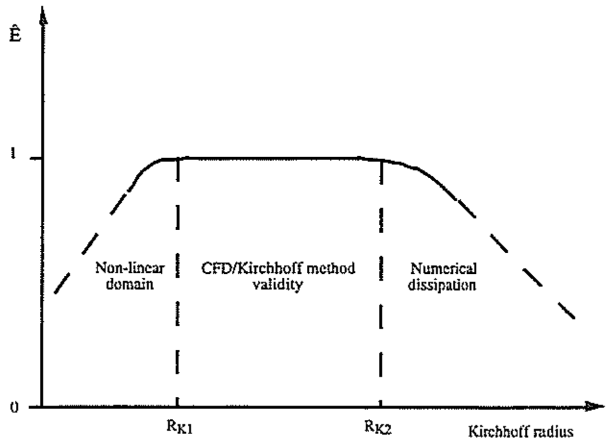

Figure 1 : Theoritical valididy domain for the Kirchhoff method

Codes

The codes and the method have already been presented in [8].

The CFD code, FP3D [9], solves the Unsteady Full-Potential equation for an isolated blade, using an implicit finite-difference algorithm in the relative frame linked to the blade. The Kirchhoff code, KARMA, computes the acoustic pressure given by the Kirchhoff integral using a fixed (non-rotating) surface formulation in the convected helicopter frame (wind tunnel configuration).

The aerodynamic data needed by the Kirchhoff code are the perturbation pressure and the perturbation pressure gradients on the control surface. The pressure is a direct output from FP3D. To improve the method efficiency and accuracy, a direct computation of the pressure gradients in the FP3D code was added, using tensor analysis. The Kirchhoff surface lies on a selected C-grid surface (top of Figure 2), sufficiently far from the blade tip such that non-linear effects are accounted for. The acoustic code includes a post-processor to FP3D, to transfer CFD output data from the rotating frame, for which grid points are not equally spaced in azimuth, to the nodes of the fixed grid of the control surface, where a constant azimuthal spacing is used (bottom of Figure 2). This is done by using a 2D bilinear interpolation program.

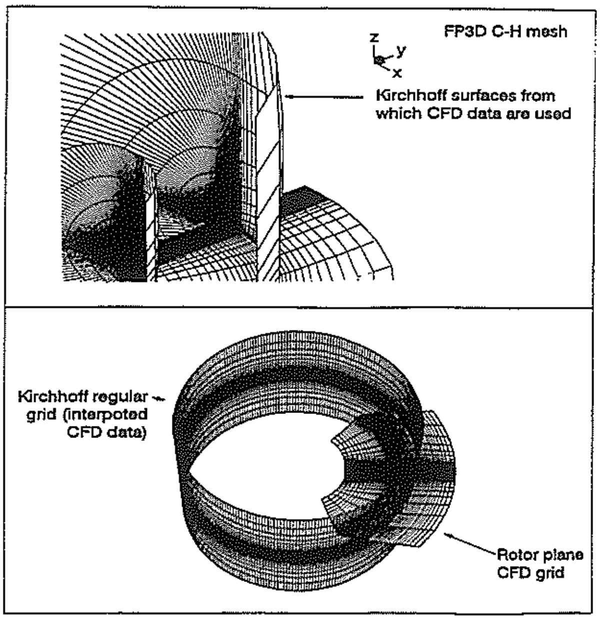

Figure 2 : Kirchhoff surface and KARMA grid

Test Conditions

The method is checked on two delocalized configurations relative to two rectangular bladed rotors tested in wind tunnels [10, 11]. The advancing tip Mach number M_{tip}, is identical for both cases which allows for a Mach similitude running. Rotors geometry and test conditions are the following:

• A two-bladed non-lifting ONERA model rotor (1.5 m diameter and 0.158 m chord), called F00 in this study. $M_{tip} = 0.9$ - $\mu = 0.4$ - Microphone located at 4 R in the rotor plane and the advancing direction.

• A four-bladed lifting model rotor (4.2 m diameter and 0.14 m chord), called 7A. $M_{tip} = 0.9$ - $\mu = 0.4$ - Microphone located at 3 R in the rotor plane and the advancing direction.

Grids

• CFD grids

The CFD grids used in this study are non adapted with respect to shock wave propagation. The mesh in the shock regions, although the radial distribution of the shock waves is curved [6, 12], is refined along straight lines within leading and trailing edge extension.
However, in order to get a large number of C-grid for an accurate parametrical study on the Kirchhoff surface position, the CFD meshes have been refined in the spanwise direction. Stability conditions relative to the cell growing rate and to the mesh size are required to insure the convergence of the scheme and to not modify the aerodynamic solution. First results obtained from previous computations on non refined grids [8] were used in this way to compare the acoustic solutions performed for the same selected Kirchhoff surface position, $R_k = 1.2$ R.
The grids used in this paper are defined by 141x50x21 nodes in the X, Y, Z directions (I, J, K indices of C-H grid) and extend from 0.5 R to 1.7 R along Y and from -10 chords to +10 chords along Z. The extent for X is ±1.37 R and ± 0.8 R respectively for the F00 and 7A rotors. The rotor plane meshes are shown in the Figure 3 (the border-cells (I_{max}, J_{max}) are not plotted). The selected Kirchhoff surfaces for the acoustic computations are plotted in dotted line and respective Kirchhoff radius value is indicated.

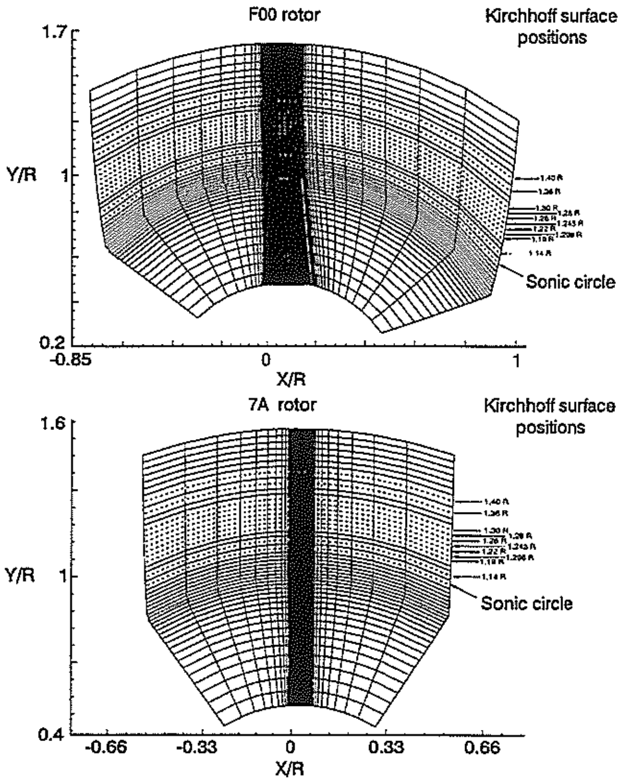

Figure 3 : CFD grids in the rotor plane

• Kirchhoff grids

The active Kirchhoff surface is an open cylinder limited between blade azimuths 15 degrees to 255 degrees due to the fact that out of this domain the acoustic sources can be neglected. The regular azimuthal spacing of the acoustic grid, $\Delta\theta$, is equal to 0.3 degree (1200 points per rev.) which roughly corresponds to the experimental acoustic sampling rate (1024 points per rev.). The vertical spacing is chosen to correspond to the aerodynamic one at the trailing edge.

Remark:

Because of algorithm simplicity and short time computation for Kirchhoff integral computation (120 sec CPU on CRAY/YMP), the time step (although it could probably be increased without loosing accuracy) is put constant and equal to $\Delta\theta/\Omega$. Thus, FP3D output data (pressure and pressure gradients) are stored every 0.3 degree.

Checking of normal pressure perturbation derivative ($\partial p/\partial n$) on the Kirchhoff surface

• $\partial p/\partial n$ term contribution on overall acoustic signature

The normal derivative of the pressure perturbation is the most contributing term to far-field noise radiation [1, 7]. This is shown in Figure 4 which compares the contribution of each Kirchhoff integral source term to the overall acoustic signature radiated at 4 R. The pressure term contribution can be neglected. The effect of time derivative term is to balance the overall signature, given by the term $\partial p/\partial n$, with respect to negative and recompression peak amplitudes. This is the reason why it is important to control this input data (much more than the pressure itself).

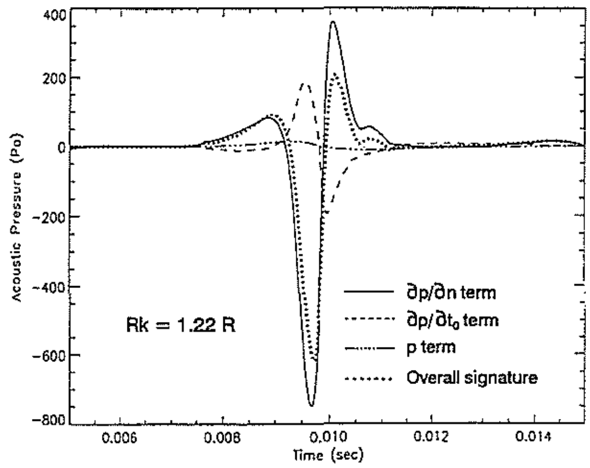

Figure 4 : Kirchhoff integral terms contribution

• Iso-$\partial p/\partial n$ contour plots : virtual sources spreading, boundary reflections and correlation with predicted noise signatures

An efficient way to check the normal derivative of the perturbation pressure is to perform iso-contour maps on a selected Kirchhoff surface for some interesting blade azimuths. This aims to control the spreading of these virtual sources.

Figures 5 and 6 show typical results obtained for three azimuths (60, 90, 105 degrees) on a Kirchhoff surface located at 1.22 R, respectively for the F00 and 7A blades. These maps are related to acoustic signatures computed by increasing the vertical extent of the integration domain, given by the k-line values, from $k_{max} = 14$ up to $k_{max} = 17$. Experimental signature is cross overplotted.

In the first case (Figure 5), the intensity of the virtual sources gradually vanishes towards the boundaries, as expected by a correct modelling. The influence of vertical domain extent on acoustic signature is clearly shown. Because all the main lobes are enclosed, the result is better for $k_{max} = 16$ (the predicted signature is getting more accurate from $k_{max} = 14$ up to $k_{max} = 16$). Beyond, accuracy is unchanged ($k_{max} = 17$ compared to $k_{max} = 16$ result) which is in accordance with the iso-contour map analysis, showing that $\partial p/\partial n$ is negligeble beyond 3.5 chords. In the second case (Figure 6), probably due to numerical reflections, a "pocket" begins to appear at $\Psi = 90$ degrees from the external boundary at 10 chords under the rotor. This pocket is getting more intense and is spreading up inside the computation domain towards the rotor plane. This phenomenon is linked to the evolution of the computed acoustic signatures from $k_{max} = 14$ up to $k_{max} = 16$. The prediction is getting better for $k_{max} = 15$ because almost all sources are accounted for and input data remains accurate. When the integration domain is extended up to $k_{max} = 16$, the reflection pocket contribution is added to the rest and the solution is disturbed. According to this, the vertical extent relative to the 7A rotor has been limited to $k_{max} = 15$, which roughly corresponds to $\pm$ 5 chords.

The iso-$\partial p/\partial n$ plot shows the vertical extent of the main lobes (virtual sources) which determines the minimal axial extent of the Kirchhoff cylinder ($\pm$ 4 chords for the F00 rotor). This allows to reduce the number of Kirchhoff grid nodes without loosing accuracy. Moreover, numerical reflections on the external boundaries can be clearly detected and the reflection disturbances may be avoided by limiting the integration domain to the main lobes extent, as it has been done here.

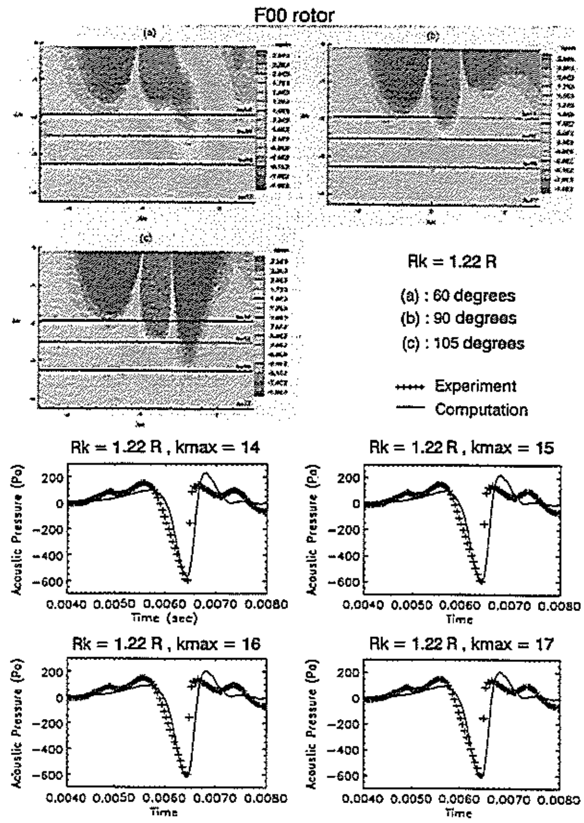

Figure 5 : Visualization of virtual acoustic sources ($\partial p/\partial n$) on the Kirchhoff surface and correlation with predicted acoustic signatures versus axial extent

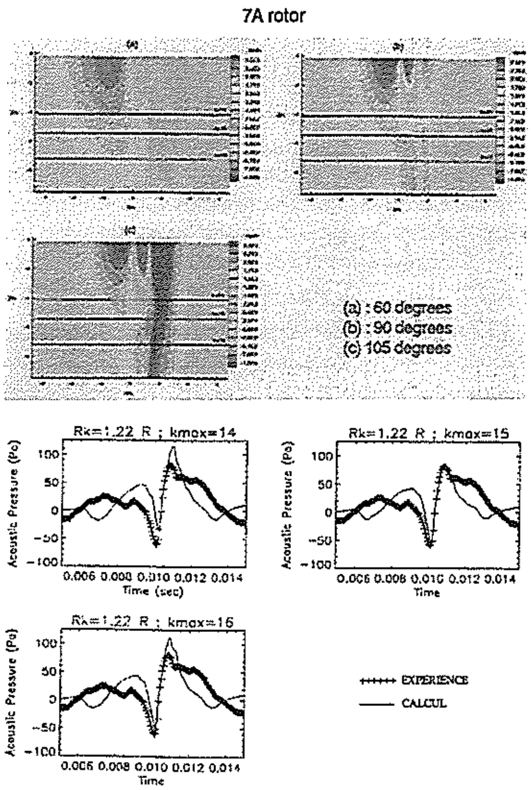

Figure 6 : Visualization of virtual acoustic sources ($\partial p/\partial n$) on the Kirchhoff surface and correlation with predicted acoustic signatures versus axial extent

Checking of the perturbation intensity in the rotor plane

• Definition of a perturbation intensity vector

In the linear acoustic theory and for a fluid at rest, the intensity vector is defined as:

$$\bar{I} = p'\bar{u}' \qquad (1)$$

$\bar{I}$ modelizes the acoustic energy flux density per time unit through an elementary surface perpendicular to $\bar{u}'$ and is expressed then in $W.m^{-2}$ (power density). In the acoustic plane wave assumption (far field noise), p' and u' are linked by the simple characteristic impedance $Z_c = \rho_0$ c. $\bar{I}$ is time and space independent on all the plane surface and can be expressed as:

$$\bar{I} = \rho_0 c\, u'^2 \bar{n} \qquad (2)$$

where $\bar{n}$ is a unit vector normal to the plane surface. Although we practically use the mean value of $\bar{I}$ for most acoustic applications, it is possible to define an instantaneous intensity vector by using the instantaneous values for p' and u'.

In the case of CFD rotor applications, non reflective boundary conditions are generally fulfilled by using directly the characteristic variables or by imposing a prescribed wave-like solution for the aerodynamic unknown. FP3D code, for the present version, uses the second approach which consists in the linearization of the potential equation using the acoustic plane wave theory [13]. The local solution is thus modelized as an outgoing plane wave which propagates normal to the cells of the external boundaries.

In order to verify the validity of these boundary conditions, an assesment of the perturbation intensity vector using the acoustic plane wave analogy has been proposed. Considering that infinite condition for the flow is given by the uniform air speed velocity U_∞, the velocity perturbation can be easily obtained by subtracting the convected terms to the overall velocity field. The pressure perturbation is classically obtained by subtracting the infinite static pressure. In the vicinity of the external boundary, these perturbations are considered to be acoustic, and intensity is computed using (1).

• Computation of I into FP3D

Using the same approach (and neglecting the velocity perturbations in the vertical direction), the instantaneous (at a given blade azimuth) perturbation intensity is computed into FP3D as:

$$\bar{I}(X,Y) = \begin{vmatrix} I_X = p\,u_X \\ I_Y = p\,u_Y \end{vmatrix}$$

where p is the perturbation pressure, and u_X, u_Y are the components of the perturbation velocity in the chordwise and spanwise directions of the convected blade frame. The modulus of $\bar{I}$ is computed as:

$$I = p\sqrt{u_X^2 + u_Y^2}$$

In the non-linear domain, although the linear acoustic theory is no valid, a perturbation intensity can be computed in the same way using the perturbation values for pressure and velocity. Neglecting the radial effects I can be related for a given blade azimuth to a theoretical expression using a small perturbations approximation [14]:

$$I \approx \rho_0 U_0 \gamma \frac{u_X^2}{c_0^2} \propto \rho_0 u_X^2 \qquad (3)$$

where U_0 is the component of the non perturbed local velocity along the blade chord. This simplified expression again shows a u^2 evolution similar to that obtained in (2) in the case of the far-field linear acoustic assumption.

• Analogy with quadrupole sources intensity

Eq. (2) and (3) can be related to the quadrupole source intensity deduced from quasi-steady calculations and conventional approximations [15, 16]. Considering only the chordwise component, for an in-plane far -field observer, the radiated Lighthill tensor T_{RR} can be simplified as:

$$T_{RR} \approx \rho_0 u_X^2$$

Since the intensity perturbation analysis can be used to verify the non reflective boundary conditions implemented in FP3D, it can be also qualitatively related (due to its analogous u^2 evolution) to the quadrupole sources distribution in the rotor plane. These two points are developed in the next section.

- Iso-intensity contour plots analysis : Source spreading, boundary reflections and correlation with predicted noise signatures

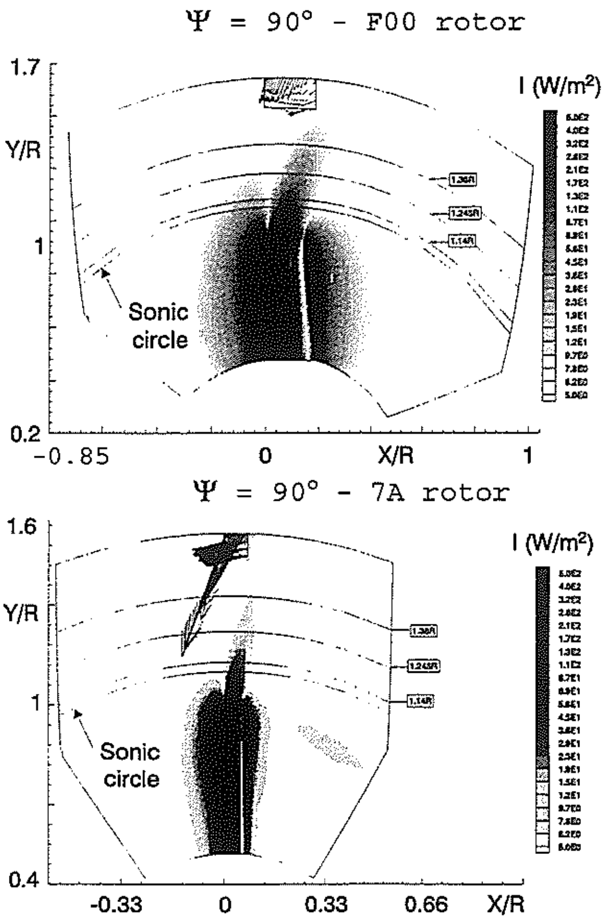

Figure 7 : Perturbation intensity in the rotor plane

The iso-I contour plots in the rotor plane, computed for each rotor at 90 degrees azimuth, are presented in Figure 7. It is well known that, for rectangular blades, this azimuth is representative for highest transonic effects and delocalization occurrence. The sonic circle and three Kirchhoff surface positions are indicated. A common scale has been chosen for the grey levels in order to distinguish the decrease of secondary lobes. Thus, the radial spreading of acoustic sources is qualitatively visualized. In particular, the shape of secondary lobes in the spanwise direction can be related to the shock curvature [12]. Intensity gradient computation along this curve could give a better estimation for main sources extent in that direction. Anyway, according to other studies [12, 15] main sources seem to vanish roughly beyond 1.25 R. In the case of the 7A rotor, a non physical "pocket" is visible downstream the trailing edge, revealing some troubles in the computation probably due to numerical reflections on the external downstream boundary. Another pocket is also detected in the 7A case on the external spanwise boundary. This phenomenon is outlined using the intensity vector plot. The length of the vector is proportional to its amplitude. The region of interest is zoomed in Figure 8.

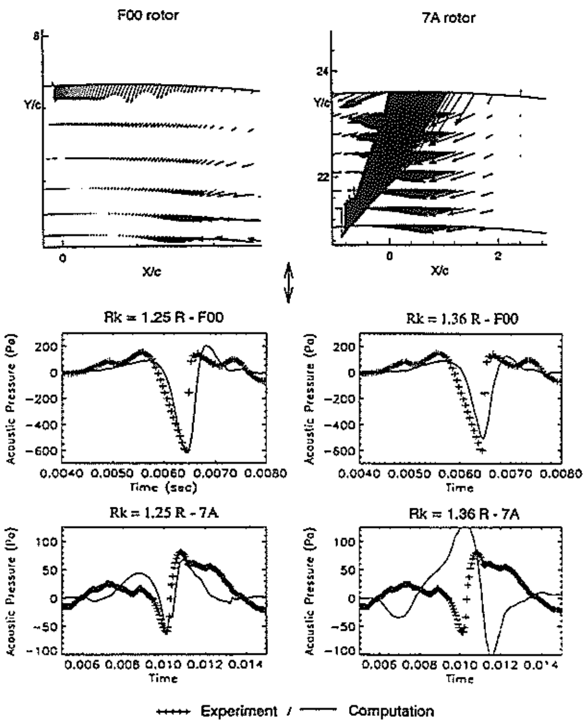

Figure 8 : Visualization of numerical reflections

At the top of this figure, two identical zoomed regions are compared. The direction of intensity vectors, incoming instead of outgoing as it is modelized in the boundary conditions (see above), reveals clearly the occurrence of numerical reflections. Since the intensity vectors are incoming in both cases, the numerical reflection effects seem negligible for the F00 case due to smooth amplitudes (no perturbation pocket was observed in the previous figure). On the contrary, because of intensity modulus high amplitudes in the 7A case, the reflections may disturb the solution up to the near-field computation domain. The effect of these numerical reflections on Kirchhoff input data accuracy is shown on the bottom of the figure which presents, for both cases, the computed acoustic signatures obtained for two Kirchhoff surfaces (R_k=1.25 R and R_k=1.36 R). For R_k=1.25 R, correlation with experiment is quite good for both cases. Removing the Kirchhoff surface to R_k=1.36R, the result relative to the 7A rotor is drastically damaged because the inputs are no longer valid. Computation to experiment discrepancies which appear on the F00 acoustic signatures are rather due to numerical dissipation effects as we will see later. The same phenomenon is also analysed in Figure 9, in which the iso-intensity maps relative to the 7A rotor have been plotted for several azimuths. These maps simulate the time evolution of intensity (acoustic sources coarsely modelized) distribution. It allows to detect the azimuth from which the aerodynamic solution becomes disturbed. In this case, at 115 degrees azimuth, the incoming reflected field is superimposed to the direct aerodynamic field so that the output data around the connected zone become non usable anymore (R_k=1.36 R result of Figure 8). For more inboard regions (R_k=1.25 R in Figure 8), output data remain accurate.

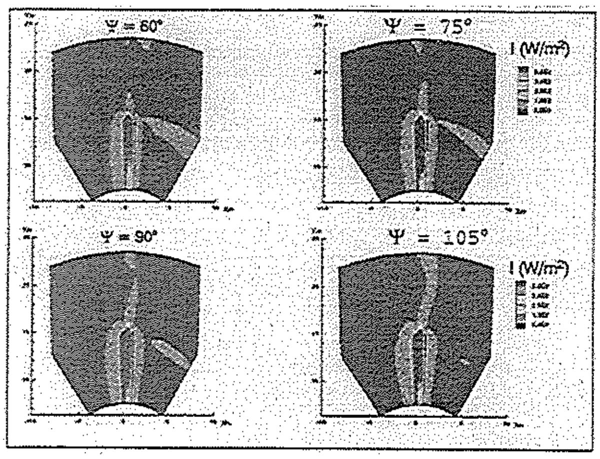

Figure 9 : Visualization of numerical reflections

Implemented in a CFD code, the computation of the perturbation intensity vector may be an efficient way to verify the validity of the outgoing wave-like boundary conditions currently adopted. It may be also used also as a pointer to estimate, through the decrease of intensity amplitude along the shock curvature, the radial extent of quadrupole sources, for a best choice of Kirchhoff surface location. According to this pointer analysis, that position is certainly comprised between 1. 2 R and 1. 3 R.

Checking of the local sound celerity in the rotor plane

• Use of local sound celerity

As we recalled in the introduction, the linear Kirchhoff formulation is valid if the control surface is put beyond the non-linear acoustic domain. The first idea to get information about acoustic non-linear domain extent is to look at the sound celerity fluctuations. Another investigation has been performed in this way.

The local celerity is computed in FP3D as:

$$c = \sqrt{\gamma \frac{p_l}{\rho_l}} \qquad (4)$$

where p_l and ρ_l are the local pressure and density.

• Order of magnitude of c/c_∞

Using isentropic relations and bernouilli equation, (4) can be written as:

$$\frac{c}{c_\infty} = \left(\frac{p_l}{P_\infty}\right)^{\frac{\gamma-1}{2\gamma}} = \left[1 + \frac{1}{2}\gamma C_p M_\infty^2\right]^{\frac{\gamma-1}{2\gamma}} \qquad (4')$$

For a stagnation point (Cp = 1 in the uncompressible fluid approximation), and M_∞ = 0.9 (which corresponds to our case when psi = 90 degrees), we obtain:

$$\frac{c}{c_\infty} \approx 1.07$$

• Iso-c/c_∞ contour plots

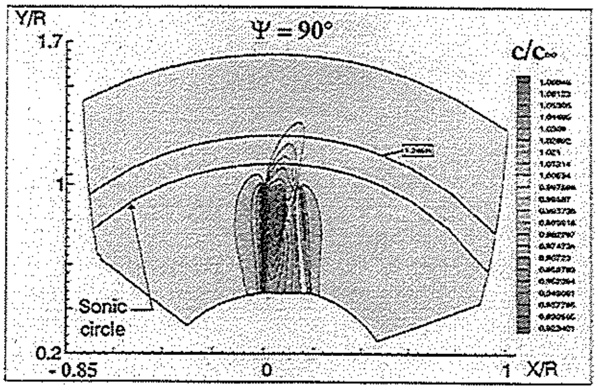

Figure 10 : Local sound celerity in the rotor plane

The iso-c/c_∞ map in the rotor plane, relative to the F00 rotor is presented in Figure 10. The maximum value obtained, c/c_∞ = 1.0695, is in very good agreement with the above approximation. The shape of the radial lobes is again representative for radial distribution of the shock. The local to infinite deviations become very small out of the blade, in the spanwise direction. On the sonic circle, the maximum deviation $(c - c_\infty)/c_\infty$ is equal to 0.89 %. The top of the last iso-contour lobe plotted in that direction indicates a deviation of only 0.25 %. These values can be analyzed by using a first order development of (4'), assuming that the perturbation pressure $p = p_l - P_\infty$ is very small compared to the atmospheric pressure P_∞ (acoustic assumption):

$$\frac{c}{c_\infty} = 1 + \frac{\gamma-1}{2\gamma}\frac{p}{P_\infty} = 1 + \frac{1}{7}\frac{p}{P_\infty} \qquad (5)$$

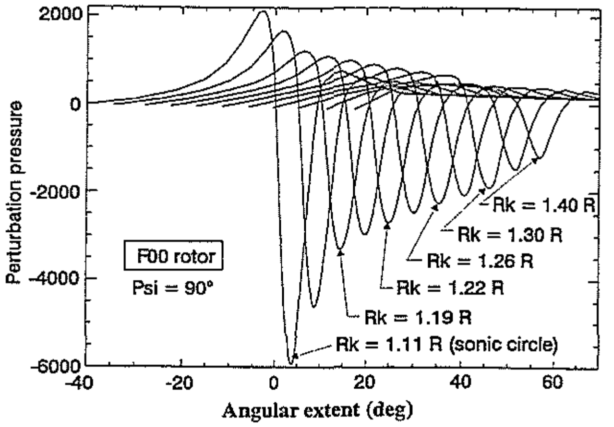

Figure 11 : In-plane perturbation pressure at several Kirchhoff radii

This approximation is used in [17] to study the acoustic non-linear effects of the sonic boom. In equation (5), c is directly deduced from p, which is a direct Kirchhoff input. The perturbation pressure signature in the rotor plane computed by FP3D is plotted for several radial station (corresponding to the selected Kirchhoff surfaces), and for $\Psi = 90$ degrees, in the Figure 11. Introducing the negative peak value for p in (5), we can compare the c/c_∞ maximum deviations obtained for some radial stations to those computed into FP3D using (4). We get smaller fluctuations with (5) near the blade tip. These gaps can be attributed to high non-linear effects in this region for which second order terms are non negligible. However, these predictions are getting closer to each other with the distance to the rotor hub and tend to converge very quickly. At the sonic circle $\Delta c/c_\infty$ is equal to 0.85 % (with (5)) instead of 0.89%. Beyond the sonic circle, Eq. (4) and (5) are roughly equivalent, giving for R_k=1.2 R, an identical $\Delta c/c_\infty$ of only 0.36 % (p/p_∞ = 0.25 %). Far away, considering the ratio p/p_∞ is small enough, the local celerity fluctuation is probably not significant anymore. It is not easy to determine accurately a minimum deviation value behind which the first order term in (5) can be neglected (c # c_∞), assuming the acoustic linear domain is reached. For this reason, this threshold value will be estimated through the analysis of far-field predicted acoustic signatures versus R_k, compared to experimental ones. This is done in the next section.

Correlation between output data analysis and computed acoustic signatures versus R_k

In order to complete the CFD data analysis and to ensure their reliability, acoustic signatures have been computed for both rotors and for each control surface location, and correlated to experiment. Comparisons are presented in Figures 12 and 13, for some selected Kirchhoff radii.

These results are summarized in Figure 14, in which the theoretical to experimental level deviations (in dB) are plotted versus the Kirchhoff radius. This graph clearly shows the limits for the validity of the method which have to be related to the theoretical graph of Figure 1. The validity domain is indicated by arrows. The limits of this domain take also into account the accuracy of the shape (particularly for the slopes) of the predicted acoustic signatures compared to experimental ones.

The method is very accurate when the Kirchhoff surface is located nearly at 1.2 R. As expected by FP3D output data analysis (perturbation intensity and local sound celerity), it is quite probable that main non-linear effects and main acoustic sources are accounted for. We can consider then that a threshold of 0.4% for local to infinite celerity deviation $\Delta c/c_\infty$ (corresponding to a ratio p/p_∞ of 0.3%) is safe enough to ensure the accuracy of the present method. Unfortunately, the range of validity is too reduced, mainly for the 7A rotor computations. Although the integration extent has been optimized (see section "Iso-$\partial p/\partial n$ contour"), the perturbation intensity maps have revealed some numerical reflections on the external boundaries of the grid. In the 7A case, the aerodynamic solution is disturbed by these reflections if the control surface is put beyond 1.25 R. In the F00 case, the method is valid up to 1.3 R. Beyond, the CFD solution is not accurate enough due to numerical dissipation which also affects the output data. The numerical dissipation was not expected to occur at so small spanwise extent, and was not detected by the output data analyses presented above.

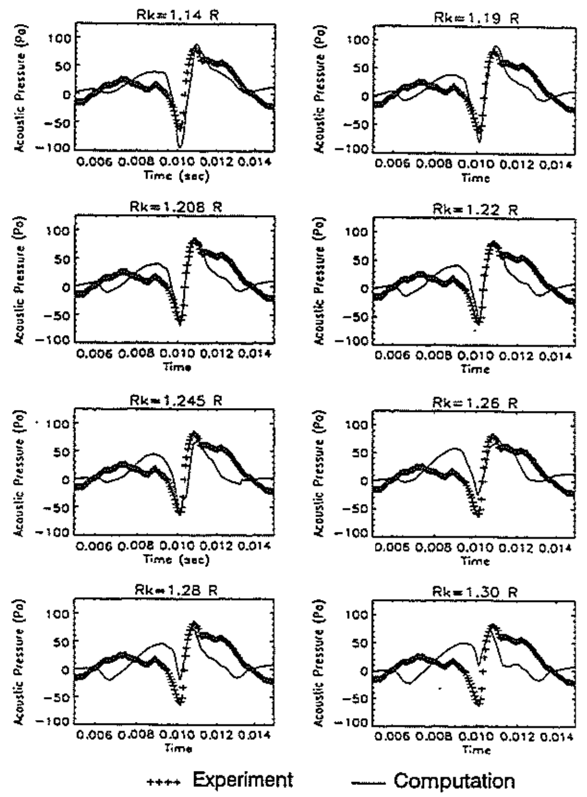

Figure 12 : 7A rotor computed acoustic signatures

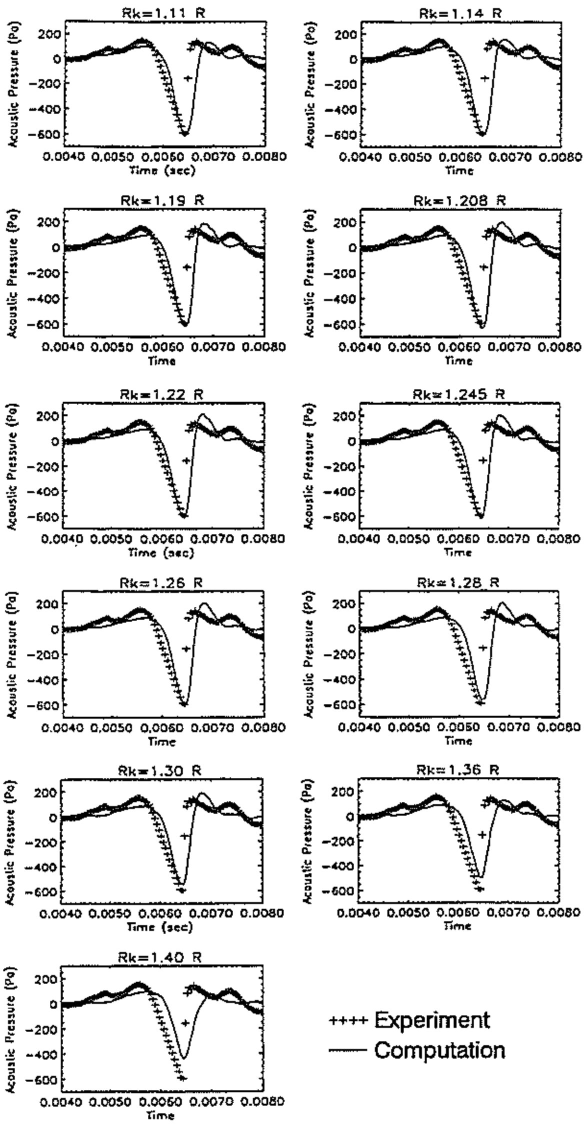

Figure 13 : F00 rotor computed acoustic signatures

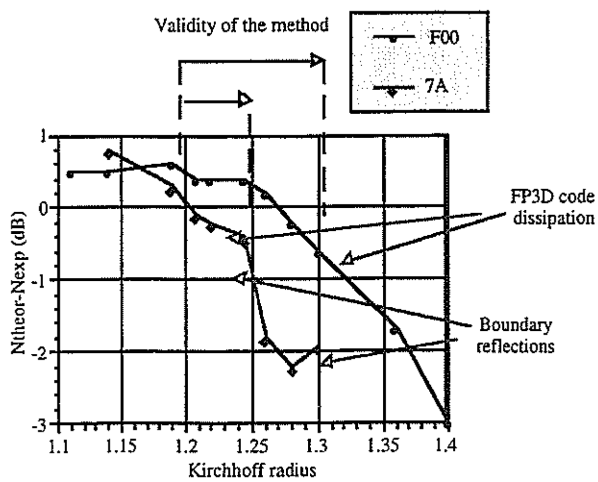

Figure 14 : Validity domain of the present CFD/Kirchhoff method

Conclusion

Control of CFD output data using simple and efficient criterion have been proposed in this paper, in order to ensure the validity of acoustic prediction using a CFD/Kirchhoff method. The checking of the perturbation pressure gradient, using iso-contour maps on a selected Kirchhoff surface, allows for a well suited size of the Kirchhoff domain integration, in particular for the vertical extent. It can also be used to detect numerical reflections at the external boundaries of the mesh as it was done here. In this way, a safe axial extent of ± 4-5 chords (since the CFD grid extent was ± 10 chords) has been obtained.

Based on an acoustic plane wave analogy, a perturbation intensity vector calculation has been proposed for a similar analysis in the rotor plane. Vector direction is used to control the non reflective boundary condition implemented in FP3D code. Thanks to this approach, numerical reflections have been clearly visualized and related to Kirchhoff inputs accuracy. Moreover, an analogy with the quadrupole sources intensity was used to simulate qualitatively the acoustic source distribution in the rotor plane.

The computation of the local sound celerity has been also implemented into FP3D. Local to infinite celerity deviations have been analysed using simple isentropic relations and first order approximations. It allows us to estimate the extent of the acoustic non-linear domain, defining the limit of the Kirchhoff surface location for linear Kirchhoff formulations currently adopted. According to the analysis of the predicted acoustic signatures computed for each selected control surface and compared to experiment, a threshold relative deviation $\Delta c/c_\infty$ of 0.4 % seems to be small enough to assess the linear acoustic assumption.

Finally, the present method with respect to Kirchhoff surface radial location is very accurate when the surface is located around 1.2 R. According to intensity and local sound celerity analyses (using FP3D code), this radial station allows for the enclosure of main acoustic sources and non linear domain for these delocalized rectangular rotor configurations. For this Kirchhoff radius, computed acoustic signatures are fairly well correlated to measurements, sound pressure level deviations being lower than 0.5 dB. Unfortunately, the aerodynamic data get very quickly perturbed as soon as the surface is moved in the far field direction, due to the influence of significant numerical boundary reflections and dissipation effects. Beyond 1.3 R, Kirchhoff inputs are drastically damaged and acoustic predictions are no more reliable.

In a next step, similar criterion should be implemented into FP3D new versions (using more efficient boundary conditions) to test the accuracy of the aerodynamic output in the zone of interest. A suited mesh for a better fitting of the shock curvature in the spanwise direction could be also used in order to improve the Kirchhoff input accuracy and to reduce the dissipation effects in the far field direction.

References

1. Baeder, J. D., Gallman, J. M., and Yu, Y. H., "A computational Study of the Aeroacoustics of Rotors in Hover", AHS 49th Annual Forum, Saint-Louis, Missouri, May 1993.

2. Lyrintzis, A. S., "Review : The Use of Kirchhoff's Method in Computational Aeroacoustics", Journal of Fluids Engineering, Vol. 116, pp. 665-676, December 1994.

3. Strawn, R.C., and Biswas, R., "Computation of Helicopter Rotor Acoustics in Forward Flight", 19th Army Science Conference, Orlando, Florida, June 1994.

4. Polacsek, C., Prieur, J., "High-Speed Impulsive Noise Computations in Hover and Forward Flight using a Kirchhoff Formulation", 16th AIAA Aeroacoustics Conference, Munich, Germany, June 1995.

5. Kuntz, M., "Rotor Noise Predictions in Hover and Forward Flight Using Different Aeroacoustic Methods", AIAA paper n°96-1695, 1996.

6. Srinivasan, G. R, Baeder, J. D., "Recent Advances in Euler and Navier-Stockes Methods for Calculating Helicopter Rotor Aerodynamics and Acoustics", 4th International Symposium on Computational Fluid Dynamics, California, 1991.

7 Zibi, J., Polacsek, C., Kuntz, M., Rouzaud, O., "Helicopter Rotor Noise Predictions Using ONERA and DLR Euler/Kirchhoff Methods", Accepted for the AHS Specialist's Meeting for Rotorcraft Aerodynamics and Acoustics, Williamsburg, Virginia, October 1997.

8. Polacsek, C., Costes, M., "Rotor Aeroacoustics at High-Speed Forward Flight Using a Coupled Full Potential/Kirchhoff Method", 21th ERF, St Petersburg, Russia, September 1995

9. Beaumier, P., Costes, M., Gaveriaux, R., "Comparison between FP3D full Potential Calculations and S1 Modane Wind Tunnel Tests Results on Advanced Fully Instrumented Rotors", 19th ERF, Cernobbio, Italy, September 1993.

10. Prieur, J., "Experimental Study of High-Speed Impulsive Rotor Noise in a Wind Tunnel", 16th ERF, Glasgow, September 1990.

11. Polacsek C., Lafon P., "High-Speed Impulsive Noise and Aerodynamic Results for Rectangular and Swept Rotor Blade Tip Tests in S1 Modane Wind Tunnel", 17th ERF, Berlin, September 1991.

12. Prieur, J., Costes, M., Baeder, J. D., "Aerodynamic and Acoustic Calculations of Transonic Nonlifting Hovering Rotors", AHS Journal, Vol. 41, 2, pp 17-26, April 1996.

13. Costes, M., Beaumier, P., Bettschart, N., Gardarein, P., "Aerodynamic Computations Applied to Helicopters", La Recherche Aérospatiale, n° 3, 167-184, 1995.

14. Desopper, A., "Helicopter Aerodynamics II", University of Maryland, Department of Aerospace Engineering, ENAE - 632, 1986.

15. Schmitz, F., H., and Yu., Y. H., "Transonic Rotor Noise - Theoretical and Experimental Comparisons", Vertica, Vol. 5 (1), pp. 55-74, 1981.

16. Prieur, J., "Calculation of Transonic Rotor Noise Using a Frequency Domain Formulation", AIAA Journal, Vol. 26 (2), pp. 156-162, February 1988.

17. Plotkin, K., J., "Review of Sonic Boom Theory", AIAA paper n°89 -1105, San Antonio, TX, April 1989.